On-Board Reagent Storage and Release by Solvent-Selective, Rotationally Opened Membranes – A Digital Twin Approach

Jens Ducrée

School of Physical Sciences, Dublin City University, Glasnevin, Dublin 9, Ireland, email: jens.ducree@dcu.ie

Abstract

Decentralized bioanalytical testing in resource-poor settings ranges among the prime applications of microfluidic systems. The high operational autonomy in such point-of-care / point-of-use scenarios requires on-board stored liquid reagents, which need to be safely contained during long-term storage, transport and handling, and reliably released prior to activation. Over the recent decades, centrifugal microfluidic technologies have demonstrated the capability of integrated, automated and parallelized sample preparation and detection of bioanalytical protocols. This paper introduces a novel concept for onboard storage of liquid reagents which can be delivered in a well-defined manner by a rotational stimulus of the system-innate spindle motor, while still aligning with the conceptual simplicity of such "Lab-on-a-Disc" (LoaD) concepts. The reagent storage technology is captured by a digital twin which allows making complex performance analysis and algorithmic design optimization according to given objectives as expressed by target metrics.

Introduction

The automation of bioanalytical assay panels has been a paramount objective of microfluidic technologies since their debut in the early 1990s [1-5]. In the meantime, these Lab-on-a-Chip devices have pervaded manifold application spaces, primarily in biomedical point-of-care and global diagnostics, liquid handling automation for the life sciences, process analytical techniques and cell line development for biopharma, as well as monitoring the environment, infrastructure, industrial processes and agrifood [6-11]. Their compliance with the relevant workflows, infrastructure, operator skill and competitive cost of ownership / per test are vital for deployment in locations outside sophisticated medical infrastructure.

Various miniaturized liquid handling platforms have been introduced, which may be distinguished by their pumping scheme; among them are pressure sources, capillary force, electrokinetics, electrowetting on dielectric, bulk and surface-acoustic waves. Throughout the last three decades, centrifugal microfluidic platforms have been at the center of commercial and academic endeavors. Driven by a rugged spindle motor, these conceptually simple "Lab-on-a-Disc" (LoaD) systems [12-35] excel through their high-performance centrifugal sample preparation solely actuated by a conventional spindle motor

Mostly operating in batch-mode, biosamples are preconditioned through a series of centrifugally implemented Laboratory Unit Operations (LUOs), such as metering [36, 37], mixing [38-41], incubation, purification / concentration / extraction [42, 43], homogenization [44, 45], particle filtering [46-51], and droplet generation [52-54], while transiently held back in each step by a downstream

valve. Note that some assay steps may also be realized by transferring functionalized magnetic particles between reagent chambers [55, 56].

Akin to the pick-up heads familiar from digital data storage technologies like CD, DVD or Blu-ray, most detection schemes for LoaD systems are based on optical detection [22-24, 57-74]. While the radially directed, outwards pointing centrifugal field is independent of the outer contours of the microfluidic chip, a disc shape complies with the rotational symmetry and supports mechanical balance, layout, and mold flow in common mass manufacturing such as (compression-)injection molding; yet, deviations from the common 12-cm diameter and 1.2-mm thick CD format have been implemented, e.g., smaller "mini-discs", tubes, or rectangular microscope slides. Furthermore, the alignment of the inlet ports, outlets and detection chambers may also be important for seamless interfacing with standard well plate-formats, liquid handling robotics, and associated equipment like readers. For better readability, we refer to all these LoaD variants as "discs" in the following.

Liquid volumes concurrently residing on a rotor experience the same spin rate, and are thus simultaneously exposed to the rotationally induced centrifugal field, which further depend on their individual radial coordinates. Hence, and other than for most conventional Lab-on-a-Chip systems, valving represents a key ingredient for automating sequential liquid handling protocols of the LoaD. In principle, the disc could be halted for valve opening, for instance, by a manual or instrument-based, e.g., mechanical, thermal or radiation-based actuator [75-83]. However, it is usually preferrable to keep the disc-based liquid volumes at bay by at least moderate centrifugation, which requires a co-rotating power source, e.g., through pneumatic pumps [84, 85] or electro-thermal or radiative units for melting sacrificial barriers film [83, 86, 87].

However, this work focusses on rotationally controlled valving concepts, which have been chosen by many researchers due to their smooth alignment with the low complexity of the LoaD platform. In these passive valves, the centrifugal pressure head driving liquid segments towards the disc perimeter is combined with other pressure contributions which are independent of external power. In their high-pass variants, the centrifugal driving force is opposed by a capillary barrier, while low-pass siphons typically feature hydrophilic coatings in inbound sections or pneumatic effects, so that valving is ushered by reducing the spin rate below a critical threshold. Also, various centrifugo- or thermo-pneumatic flow control mechanisms [88-97] have been elaborated to create forward or reverse pressure differentials.

To provide full-fledged sample-to-answer automation in compliance with point-of-care applications, the disc has to be pre-loaded with liquid or dry reagents, to avoid managing the logistics and loading from separate stocks; the user then only needs to introduce the sample into the disc. As opposed to many concepts conceived for temporarily retaining liquid volumes while carrying out LUOs along liquid handling sequences, reagent valves need to impede diffusion or exposure to ambient humidity over a shelf lives of months to years, and possibly rough handling during transport.

Various concepts based on physical barriers, like pouches, cartridges or wax plugs, have been developed; similar to the previously discussed active valves, these containers may be opened by stimuli such as mechanical piercing, illumination by a high-power laser, or by local heating. Essential performance criteria are their compatibility with requirements of manufacture and assembly, evaporation, absorption into the bulk material, and possible leaching of chemicals during extended contact. Furthermore, the reliability of the release mechanism and the accuracy, precision and recovery ratio of the stored liquid volume need to be accounted for.

Dovetailing the centrifugal microfluidics covered in this work, also rotationally induced opening has been demonstrated. For these concepts, it needs to be considered that, e.g., for limited motor power and safety, there is an upper limit for practically achievable spin rates, and the reservoir might have to be placed centrally, which would severely restrict obtainable pressure heads to fractions of common atmospheric pressures. Thus, the reservoir valve has to yield at rather small pressure heads. Furthermore, the mechanical strength of a designated weak point is hard to define, thus smearing out the associated spin rate threshold for release. Operational reliability hence demands setting a high spin frequency for release, which tends to counteract the options for fluidic multiplexing of concurrently loaded liquids [85].

This paper focuses on a novel type of rotationally actuated valve; during storage of an aqueous reagent, a (water) dissolvable film (DF) presents a diffusion barrier which is initially protected by an oleophilic, ancillary liquid having a certain, specific density [50, 75, 96, 98-100]. Upon spinning, a centrifugo-hydrostatic equilibrium is reached in which the interface between the two immiscible liquids contacts and thus dissolves the DF. In an idealized model, the reagent will be released at any finite spin rate.

In addition to the general prerequisites for on-board storage of liquid (and potentially also for protecting dry / lyophilized) reagents, such valves need to meet further specifications. During logistics and manual handling, acceleration due to shaking and terrestrial gravity act on the liquid volumes, while the meniscus between the immiscible fluids needs to stay near its default rest position to avoid premature opening. Furthermore, manufacturing and dispensing precision, evaporation rates, and structural fidelity affect the release mechanism, and potentially enclosed or emerging gas bubbles need to be tolerated.

This work first elaborates the operational principles for these rotationally controlled on-board storage and release valving. Then strategic features of the basic layout are introduced, and first motivated in a mostly qualitative manner. Next, key performance indicators (KPIs) are defined as design objectives, which are individually or collectively optimized along the “digital twin” derived from the underlying functional model.

Working Principle

Figure 1 illustrates the fundamental mechanism underpinning storage and release of liquid reagents. In the portrayed, exemplary fluidic structure, which is referred in the following to as Γ, two reservoirs of upper and lower cross sections A and a, and heights H and h on the left, and A' and a', and H' and h' on the right, hold the aqueous reagent and the immiscible ancillary liquid of densities ϱ and ϱ', respectively. These containers are interconnected by an isoradial channel at an inner radial position R of axial length $\mathcal{L}$, radial height $\mathcal{H}$, and of cross section $\mathcal{A}$, which accommodates a water-dissolvable film of axial extension δZ at the (mean) position $\mathcal{Z}$ on the z-axis.

For storage and transport ($\omega = 0$), the phase interface between the immiscible liquids is to reside within a (coaxial) segment of a cross section a of axial length δz, at a target position $z = z$, or at least $|z - z| \leq 0.5 \cdot \delta z$. For activation and release in hydrostatic equilibrium at an angular spin rate at $\omega = 2\pi \cdot \nu > 0$, the meniscus needs to move beyond the DF at $z = \mathcal{Z}$.

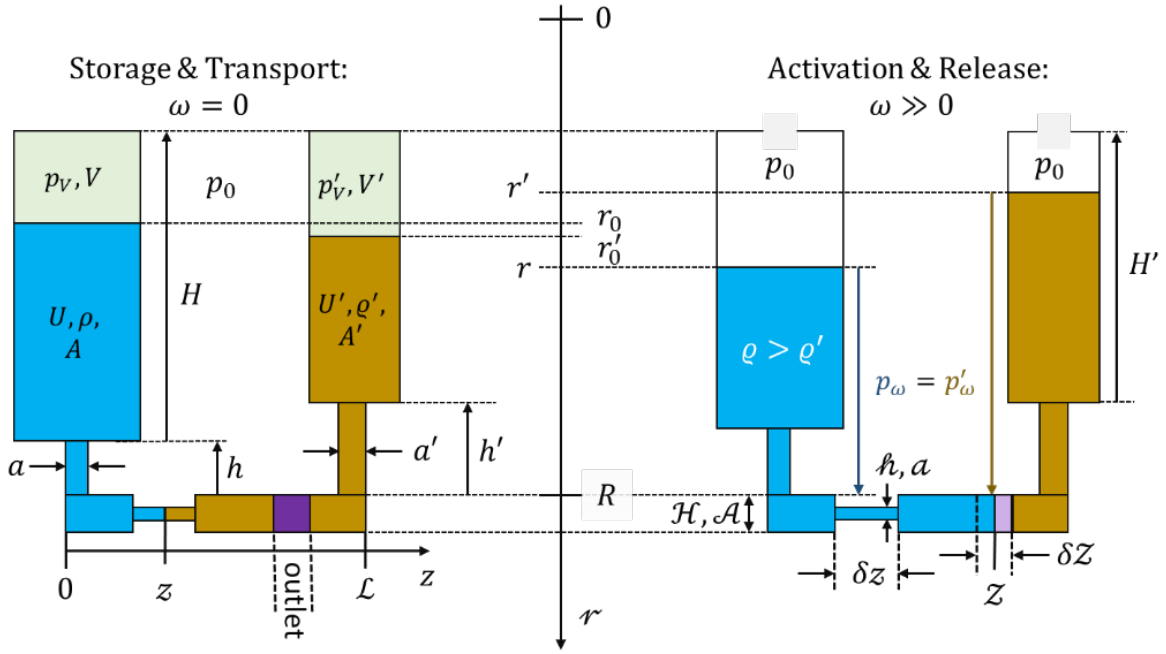

Figure 1 Basic storage and release mechanism (linearized, 2-dimensional display of cylindrical coordinates, dimensions not to scale). The two-pronged structure, referred to as Γ, is divided into upper and lower radial sections of cross sections A and A', and a and a', and heights of H, H', h and h', respectively. An isoradial channel at an inner radial position R possesses an axial length $\mathcal{L}$, a radial extension $\mathcal{H}$ and cross section $\mathcal{A}$; a section of radial height $\hbar$ and cross section a and length $\delta z < \mathcal{L}$ is centered at z to provide a further degree of freedom. (Left) In a first step at rest ($\omega = 0$), the aqueous reagent and an immiscible ancillary liquid of volumes U and U', densities ϱ and ϱ', and viscosities η and η', are loaded to the left and right reservoirs with meniscus positions r_0 and r_0' of their liquid distributions $\Lambda(\omega)$ and $\Lambda'(\omega)$, respectively; their phase interface z is targeted to be located within the center of the $\mathcal{Z}$-segment centered at $z = \mathcal{z}$ in the isoradial channel, or at least $|\tilde{z} - \mathcal{z}| \leq 0.5 \cdot \delta\mathcal{Z}$. These compartments are then isolated at pneumatic pressures $p_V(\omega = 0) = p_V'(\omega = 0) = p_0$ (9) from the ambient pressure to $p_0 \approx p_{\text{std}} = 1013.25$ hPa. (Right) Before its (default) on-site usage, both seals are removed from the disc. During rotation at (theoretically any) $\omega > 0$, the initial difference $\Delta p_\omega(\varrho, \varrho', U, U', R, \Gamma, \omega, z) = p_\omega(\varrho, U, R, \Gamma, \omega, z) - p_\omega(\varrho', U', R, \Gamma, \omega, z) > 0$ resulting from the pressure heads p_ω (4) drives the liquid distributions $\Lambda(\omega)$ and $\Lambda'(\omega)$ towards hydrostatic equilibrium $\Delta p_\omega(\varrho, \varrho', U, U', R, \Gamma, \omega, z) = 0$ (4), and consequently new inner meniscus positions $r > r_0$ and $r' < r_0'$. For triggering the reagent release through an outlet, e.g., located in a lower disc layer connected by a vertical via, the liquid-liquid interface at $z = z(\varrho, \varrho', U, U', R, \Gamma, \omega)$ in hydrostatic equilibrium needs to cover the DF at $z = \mathcal{Z}$ having an axial extension $\delta\mathcal{Z}$ that was so far protected by the ancillary liquid, i.e., $z \geq \mathcal{Z}$. Note that the geometry Γ is composed of cuboid segments to facilitate calculations. The default values for the parameters indicated are compiled in Table A1. Evidently, by suitably adjusting the dissolution characteristics of the DF, also non-aqueous liquids may be stored and released with the same mechanism.

The conservation of liquid volumes is generally expressed as

$$U(\check{r}, \hat{r}) = \int_{\check{r}}^{\hat{r}} A(r) dr \tag{1}$$

for general geometries Γ by the integral over the function $A(r)$ representing the dependence of the (partially compartmentalized) cross section A on the radial coordinate r between the inner and outer radial confinements of the liquid distributions Λ or Λ'; this liquid volume U (1) spans between its inner and other radial confinements $\check{r}$ and $\hat{r}$, respectively.

To simplify calculations without compromising the outcomes of this work, we consider a structure Γ composed of cuboidal segments in Figure 1, with $\check{r} = r_0$ or r, and $\hat{r} = R + \hbar$. Instead of having to (numerically) solve the possibly complex integral $U(\check{r}, \hat{r})$ in (1), the liquid volumes can then be calculated (assuming $R - h - H \leq r \leq R - h$) by the algebraic formulas

$$U = A \cdot (R - h - r) + a \cdot h + \mathcal{A} \cdot z \Rightarrow r = r(U, R, \Gamma, z) \tag{2}$$

for the aqueous reagent and (assuming $R - h' - H' \leq r' \leq R - h'$)

$$U' = A' \cdot (R - h' - r') + a' \cdot h' + \mathcal{A} \cdot (L - z) \Rightarrow r'(U', R, \Gamma, z) \quad (3)$$

for the ancillary liquid. Equations (2) and (3) link the loaded liquid volumes U and U' to the radial position R of Γ, its structural parameters $A, A', a, a', h, h', \mathcal{A}, \mathcal{a}, \mathcal{z}, \delta\mathcal{z}$ and $\mathcal{L}$ as represented by Γ, and the interface at $0 < z < \mathcal{L}$; the liquid levels at rest can therefore be expressed as $r = r(U, R, \Gamma)$ in (2) and $r'(U', R, \Gamma)$ in (3).

Loading, Storage and Transport

Following a suitable, well-reproducible, possibly closed-loop controlled experimental loading procedure at $\omega = 0$, the two liquids are introduced at ambient pressure p_0 (typically $p_0 \approx p_{\mathrm{std}}$ with the standard atmospheric pressure $p_{\mathrm{std}} = 1013.25\ \mathrm{hPa}$) to place the phase interface at z within the center of the isoradial segment at $\mathcal{z}$. For a starting position $z = \mathcal{z}$ of the initial interface after properly loading U and U' at $\omega = 0$, the conservation of mass (1) trivially yields the initial filling levels $r_0 = r_0(U, \Gamma, \mathcal{z})$ and $r_0' = r_0'(U', \Gamma, \mathcal{z})$. To suppress evaporation and contamination during subsequent storage, transport and handling, the two reservoirs are then isolated from ambient by a membrane exhibiting good barrier properties.

Liquid Release

In response to spinning at a finite spin speed $\omega > 0$, the centrifugal pressure heads

$$p_\omega = \varrho \cdot \bar{r}\Delta r \cdot \omega^2 \text{ and } p_\omega' = \varrho' \cdot \bar{r}'\Delta r' \cdot \omega^2 \quad (4)$$

are induced to reshape the liquid distributions Λ and Λ', which are confined by their menisci at the radially inner r, r' and common outer positions R, respectively. (Note that $\mathcal{H}/R \ll 1$ and $\mathcal{h}/R \ll 1$ are assumed throughout.) The products $\bar{r}\Delta r$ and $\bar{r}'\Delta r'$ in (4) are composed of the mean radial positions $\bar{r} = 0.5 \cdot (R + r)$ and $\bar{r}' = 0.5 \cdot (R + r')$, and the liquid level differences $\Delta r = R - r$ and $\Delta r' = R - r'$.

In default actuation mode, the pneumatic seals are removed from the disc prior to launching the centrifugal assay protocol $\omega(t)$. While rotating at sufficiently high ω, so that $p_\omega \propto \omega^2$ (4) overcomes adverse stiction and capillary effects, a hydrostatic equilibrium

$$\Delta p_\omega = p_\omega - p_\omega' \quad (5)$$

establishes which can be rewritten

$$\varrho \cdot (R + r) \cdot (R - r) = \varrho' \cdot (R + r') \cdot (R - r') \quad (6)$$

and therefore only relates the two liquid levels $r = r(\varrho, \varrho', U, U', R, \Gamma)$ and $r' = r'(\varrho, \varrho', U, U', R, \Gamma)$ to the radial position R of Γ, the loaded liquid volumes U and U', and their densities ϱ and ϱ', but not to ω. The new, centrifugally stabilized position of the phase interface is defined by $\Delta p_\omega(\varrho, \varrho', U, U', R, \Gamma, z) = 0$ (5), and hence directly obtained from r and Γ, i.e., $z = z(\varrho, \varrho', U, U', R, \Gamma)$.

Consequently, centrifugally triggered release through the DF at $\mathcal{Z}$ comes down to $z \geq \mathcal{Z}$, which requires $\Delta p_\omega(z) > 0$ (5) during the transition of the meniscus at z all along the way from the position during storage at $\mathcal{z}$ to the DF at $\mathcal{Z} > \mathcal{z}$. This condition entails that a minimum reagent volume

$$U_\Delta(z) = \int_{\mathcal{z}}^{z} A(\mathcal{z}) d\mathcal{z} = 0.5 \cdot \mathcal{a} \cdot \delta\mathcal{z} + \mathcal{A} \cdot (z - \mathcal{z} - 0.5 \cdot \delta\mathcal{z}) \quad (7)$$

(for $\mathcal{z} + 0.5 \cdot \delta\mathcal{z} \leq z \leq \mathcal{Z}$) needs to be displaced for valve opening, and the shift of the left liquid level from r_0 to $r > r_0$, while the meniscus of the ancillary liquid moves radially inbound from r_0' to $r' < r_0'$. If all meniscus position r_0, r, r_0' and r' remain in their respective inner compartments of cross sections

A and A' during this reconfiguration towards centrifugo-hydrostatic equilibrium from $z = \mathcal{z}$ to $\mathcal{Z}$, we obtain $r = r_0 + U_\Delta(\mathcal{Z})/A$ and $r' = r_0' - U_\Delta(\mathcal{Z})/A'$.

Reliability

In practical applications, tolerances, mainly in the geometrical dimensions, as quantified by the standard deviations referred to as $\Delta\Gamma$, and in the liquid volumes ΔU and $\Delta U'$ after pipetting, impact the spread Δz of the interface z from their target positions $\mathcal{z}$ and $\mathcal{Z}$ at $\omega = 0$ and $\omega > 0$, respectively. Using (5), (2) and (3) for the meniscus position $z = z(\varrho, \varrho', U, U', R, \Gamma)$, its standard deviation

$$\Delta z(\left\{\frac{\partial z}{\partial \gamma_k}\right\}, \{\Delta\gamma_k\}) = \sqrt{\left(\sum_k \frac{\partial z(\varrho, \varrho', U, U', R, \Gamma)}{\partial \gamma_k} \cdot \Delta\gamma_k\right)^2} \tag{8}$$

depends on the values $\gamma_k \in \{\varrho, \varrho', U, U', R, \Gamma\}$, their standard deviations $\Delta\gamma_k \in \{\Delta\varrho, \Delta\varrho', \Delta U, \Delta U', \Delta R, \Delta\Gamma\}$, and the partial derivatives $\partial z/\partial\gamma_k$ evaluated at the critical positions $\mathcal{z}$ and $\mathcal{Z}$, respectively. Note that strictly speaking, equation (8) only holds for small deviations $\{\Delta\gamma_k\}$. Alternatively, as used for robustness analysis further below, Monte-Carlo methods can be employed to compute Δz at the two target positions $z = \mathcal{z}$ and $\mathcal{Z}$.

According to this fluidic model, operational robustness during storage, transport and rotation caused by statistical variations $\{\Delta\gamma_k\}$ is tightly linked to squeezing the interval of the actual interface positions $z \pm 0.5 \cdot M \cdot \Delta z$ (8) within the narrow segment after loading at rest, i.e., $M \cdot \Delta z(\omega = 0) < 0.5 \cdot \delta\mathcal{z}$, and for reliable release at $\omega > 0$, $M \cdot \Delta z(\omega > 0) < 0.5 \cdot \delta\mathcal{Z}$. The factor M quantifies the targeted degree of operational robustness, with $68\%, 95\%, 99.7\%, 99.99\%, \ldots$ for $M = 1,2,3,4, \ldots$.

Design Characterization and Optimization

The digital twin [101-103] developed here allows to configure the free experimental parameters $\{\gamma_k\}$ to achieve key performance goals, while staying commensurate with design-for-manufacture and scale-up of fabrication [104]. Underlying design optimization is facilitated by the multi-segmented structure Γ (Figure 1) featuring cross sections $A, a, A', a', \mathcal{A}$ and $\mathcal{a}$ with respect to the axial direction (and their respective axial heights / lengths $H, h, H', h', \delta\mathcal{z}$ and $\mathcal{L}$). The core motivation of this draft layout is now briefly outlined on a qualitative, heuristic manner; note that the due to the huge variety of possible application cases in the multi-dimensional parameter space $\{\varrho, \varrho', U, U', R, \Gamma\}$, only computational optimization towards well-defined target metrics will eventually provide the proper geometry.

The liquid volumes U and U' are chosen to settle the menisci r and r' in the inner (wider) region of their reservoirs with cross sections A and A' so that effects of volume deviations, whether related to systematic loss by evaporation or dispenser precision ΔU and $\Delta U'$, on the initial liquid levels r_0, and r_0', and thus the centrifugal equilibrium (5) determining z at $\omega > 0$, are mitigated. For given volumes U and U', the lower radial segments of the reservoirs display smaller cross sections a and a'; for instance, $a < A$ amplifies $\Delta r = r' - r$ entering the net pressure $p_\omega \propto \Delta r$ (4) for pumping the minimum volume fraction U_Δ (7) of U to reach $z = \mathcal{Z}$, as required for prompting disintegration of the DF.

The additional segment centered at $\mathcal{z}$ in the isoradial channel featuring a profile $\mathcal{a}$ over an axial extension $\delta\mathcal{z}$ has been introduced for supporting the definition of the liquid-liquid interface, and to suppress the shift of the meniscus by a high flow resistance scaling with $\delta\mathcal{z}/\mathcal{a}^2$ during storage and transport. Evidently, it is critical that the actual position of the meniscus at $\tilde{z}$, when factoring in experimental tolerances in $\{\varrho, \varrho', U, U', R, \Gamma, \}$, remains between the edges, i.e., $|\tilde{z} - \mathcal{z}| < 0.5 \cdot \delta\mathcal{z}$

(while avoiding enclosure of gas between the liquid phases). A large extension δz is desirable for improving the tolerance to discrepancies in the loading procedure of the two liquids.

Loading

The reservoirs are filled at the factory (at rest, i.e., $\omega = 0$) with the two immiscible liquids, in the main case considered here water and FC-72 (3M™ Fluorinert™ Electronic Liquid FC-72), of target volumes U and U' and densities ϱ and ϱ' through their designated inlet ports. The loading procedure should be highly reproducible, and ideally be monitored until the actual meniscus location $\tilde{z}$ matches z, or at least settles sufficiently central in their designated channel section around z, i.e., $|\tilde{z} - z| \ll 0.5 \cdot \delta z$.

Transport

When taken out of its storage, a LoaD may experience various accelerations β, e.g., repetitively during manual handling, walking or in a moving vehicle, or punctually and more forcefully when its full weight hits solid ground after falling from a height. The directions of the resulting, usually unintended forces tend to be random, but may possess components parallel to the designated radial axis during spinning. The unknown number, magnitude, orientation and duration of such arbitrary inertial effects make it impossible to exactly quantify their impact on the deviation of the actual meniscus position $\tilde{z}$ from its target value z. As successive accelerations might point in opposite directions, and thus neutralize their effect on the meniscus position, it is mostly likely that a single hard impact aligned in r-direction will compromise the liquid distributions Λ and Λ'. We consider here two main mechanisms for pinning the phase interface during transport.

Pneumatic Stabilization

Air-tight membranes seal the inlet ports of the reservoirs after loading the reagent and ancillary liquid to prevent evaporation. These barriers also pneumatically stabilize Λ and Λ' by virtue of Boyle's law

$$p_V = p_0 \cdot \frac{V_0}{V} \tag{9}$$

stating that a change of an originally confined gas volume V_0 at p_0 to V alters the pressure to $p_V \neq p_0$ (9). So, for instance, according to the conservation of liquid volume $dU/dt = 0$ (1), transport-related disruption may induce a shift of the liquid level r on the (left) aqueous side towards the center of rotation, which ensues a peripheral displacement of the liquid level r' of the ancillary fluid (right) towards R (Figure 1).

The resultant changes in the gas volumes V and V' lead to an increase in p_V and a reduction of p'_V, thus seeking to restore $\tilde{z} \mapsto z$. The driving pressure (difference)

$$\Delta p_V(z) = p'_V(z) - p_V(z) = p_0 \cdot \left[\frac{V'_0}{V'(z)} - \frac{V_0}{V(z)}\right] = p_0 \cdot \left[\frac{V'_0}{V'_0 - U_\Delta(z)} - \frac{V_0}{V_0 + U_\Delta(z)}\right] \tag{10}$$

should thus be maximized through adjusting the z-dependent displaced liquid volume $U_\Delta(z)$ in (7), and the initial gas volumes V_0 and V'_0 underneath the seal for stabilizing the interface position near $z = z$ during transport. Figure 2(left) illustrates the dependency of the effective counter pressure Δp_V (10) in response to (left) a shift z from the default $z = 10\,\mathrm{mm}$. Figure 2(right) reveals that the restoring pressure $\Delta p_V < 0$ (10), evaluated at the downstream boundary of the z-segment $z = z + 0.5 \cdot \delta z$, approaches 0 towards scaling the initially enclosed gas volumes V_0 and V'_0 by the (same) factor ξ.

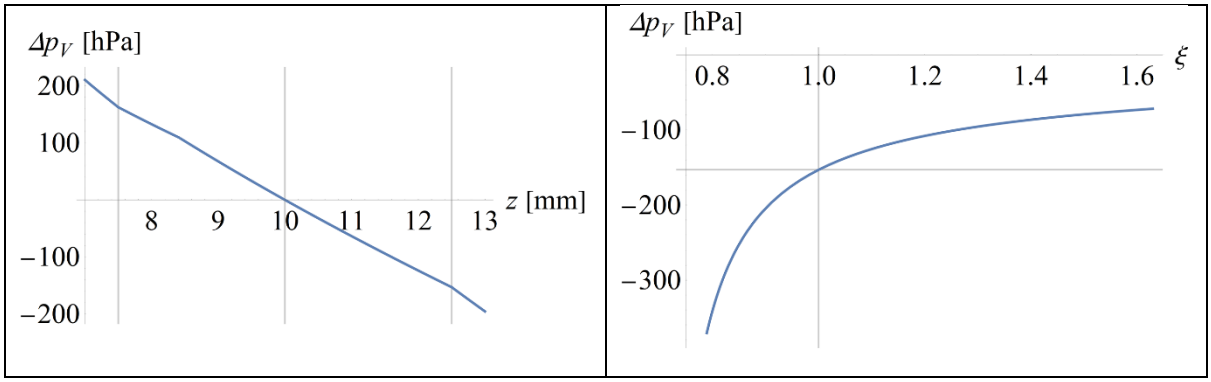

Figure 2 Net pneumatic (counter-)pressure Δp_V (10) as a function of (left) the axial coordinate z with the equilibrium $\Delta p_V = 0$ at $z = z$, and (right) scaling the initial volumes V_0 and V_0' by a by applying factor ξ to their heights while pinning the meniscus position at the end of the z-section $z = z + 0.5 \cdot \delta z$. Reducing the initial gas volumes V_0 and V_0' thus stabilizes the actual meniscus position $\tilde{z}$ in the vicinity of z during transport. Default values (Table A1) are used in this example.

Geometrical Factors

It would be operationally disastrous if the full volume $U_\Delta(\mathcal{Z})$ in (7) was displaced so that the aqueous reagent already reaches $z \geq \mathcal{Z}$ to open the DF during storage, transport and handling. This fatal event would happen when the liquid distributions Λ and Λ' have experienced an acceleration β with a strong component parallel to the radial r-direction of the centrifugal field (Figure 1) for a sufficiently long duty cycle τ. Note that even not discussed here for the sake of clarity, the interface may also leave the designated isoradial region, i.e., $z > z + 0.5 \cdot \delta z$, under the impact of β to disrupt the phase interface.

In response to an acceleration β with a major component parallel to the r-axis, the liquid distributions Λ and Λ' seek hydrostatic equilibrium (5). The resulting flow is driven by the pressure differential

$$p_\beta \approx \beta \cdot [\varrho \cdot \Delta r - \varrho' \cdot \Delta r'] \tag{11}$$

(initially) applying along the axial z-axis towards $\mathcal{Z}$, and throttled by the aggregate hydrodynamic resistance

$$\mathcal{R} = \sum_q \mathcal{R}_q = \sum_q c_q \cdot \frac{\eta_q \cdot l_q}{A_q^2} \tag{12}$$

of the structural segments indexed by q, possessing a cross section A_q, and filled over an axial length l_q with the reagent and ancillary liquid with viscosities η or η', respectively. The numerical coefficients c_q amount to 8π for a round cross section. This law of Hagen-Poiseuille delivers a volume flow rate

$$\dot{U}_V = \frac{dU}{dt} = \frac{p_\beta}{\mathcal{R}} \approx \frac{\beta \cdot [\varrho \cdot \Delta r - \varrho' \cdot \Delta r']}{\sum_q c_q \cdot \eta_q \cdot l_q / A_q^2} \tag{13}$$

which is governed by p_β (11) and $\{\mathcal{R}_q\}$ (12). As the outlet opens for $\dot{U}_V \cdot \tau \geq U_\Delta(z)$ in (7), the duty cycle $\tau = U_\Delta / \dot{U}_V$ ought to be maximized to best suppress operationally disastrous premature release of reagent during transport. However, since β in unknown, we define a resilience (evaluated for $z = \mathcal{Z}$)

$$\tau_\beta = \frac{\tau}{\beta} = \frac{U_\Delta}{\beta \cdot \dot{U}_V} \approx \frac{\sum_q c_q \cdot \eta_q \cdot l_q / A_q^2}{[\varrho \cdot \Delta r - \varrho' \cdot \Delta r']} \cdot [0.5 \cdot a \cdot \delta z + \mathcal{A} \cdot (\mathcal{Z} - z - 0.5 \cdot \delta z)] \tag{14}$$

expressed in units of $\mathrm{s}^3 \cdot \mathrm{m}^{-1}$, to be maximized by adjusting to the structure Γ (Figure 1) for mitigating adverse effects owing to transport conditions.

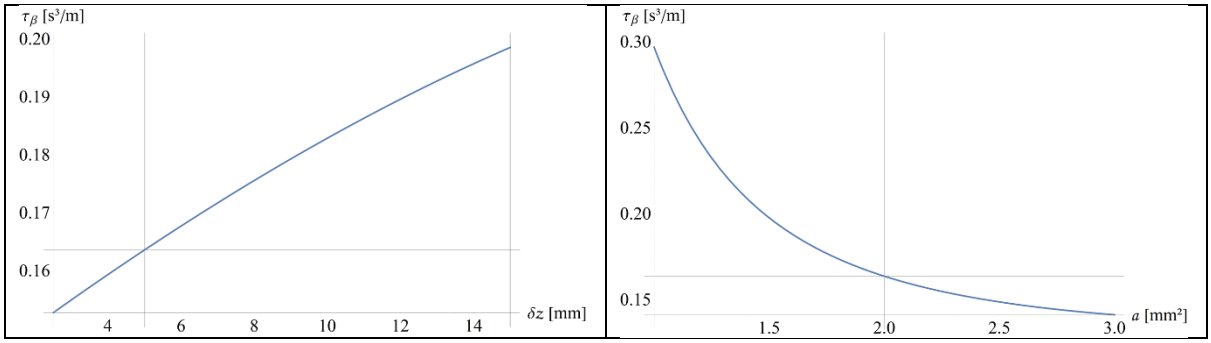

Figure 3 Resilience quantified by τ_β (14) of the liquid distributions Λ and Λ' contained in the structure Γ as a function of (left) the length $l_q = \delta z$ of the isoradial segmented centered at z, and (right) its cross section $a_q = a$. Is inferred from its definition (14), the resilience steeply increases towards high flow resistance $\mathcal{R}$ (12), i.e., with l_q/a_q^2. The gridlines mark the values when using default parameters (Table A1).

This design goal of maximizing τ_β (14) translates into maximizing the dead volumes $U_\Delta(\mathcal{Z})$ (7) of the isoradial channel extending between $z = z$ on the left side, and $\mathcal{Z}$ on the right, mostly determined via the part having the (larger) cross section $\mathcal{A}$. Furthermore, the flow rate $\dot{U}_V$ (13) should be minimized; this implies that the (initial) liquid level difference $r' - r$ should be minimized, e.g., by adjusting the cross sections or the reservoirs A, a, A' and a', while the dominant flow resistance $\mathcal{R}$ (12), as imposed by the isoradial segment of length $l_q = \delta z$ and cross section $A_q = a$, and scaling with the geometrical ratio $\delta z/a^2$, should be high. As the reagent is usually given, an ancillary liquid possessing a high viscosity η' would also be beneficial to increase τ_β (14). Figure 3 shows the dependency of the resilience τ_β (14) on (left) the length δz, and (right) the cross section a of the z-segment, which accounts for the highest impact on the flow resistance $\mathcal{R}$ (12) through $\mathcal{R}_q \propto \delta z/a^2$.

Design Optimized for Transport

By maximizing the quantities Δp_V (10) and τ_β (14) within the practical ranges of their input parameters $\{\gamma_k\}$ and their tolerances $\{\Delta\gamma_k\}$, the parametrized structure Γ can be algorithmically optimized to achieve these design goals. Figure 4 shows (left) the layouts for highest restoring pressure Δp_V (10), (center) the resilience τ_β (14), and (right) their product $\Delta p_V \cdot \tau_\beta$.

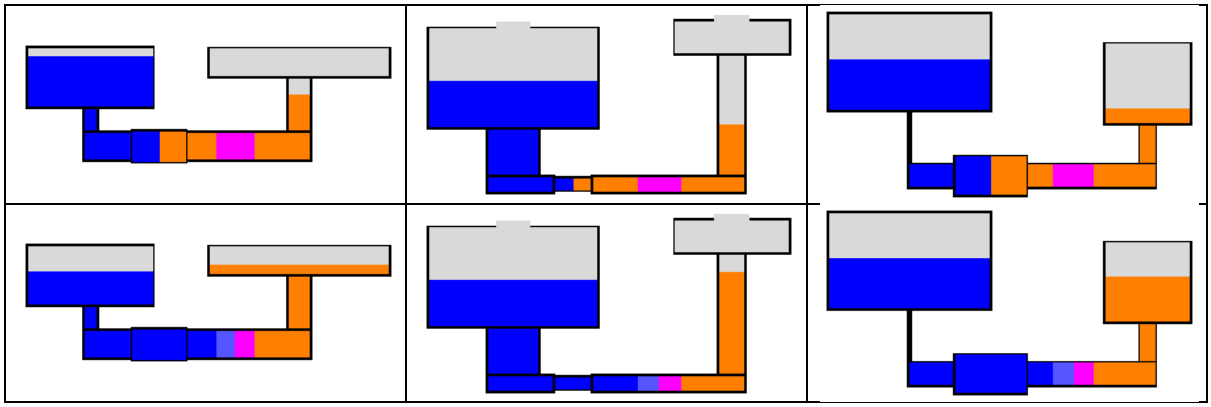

Figure 4 Algorithmically optimized layouts Γ according to given design metrics for stabilizing the liquid-liquid interface at $z = z$ during transport. (Left) Pneumatic Δp_V (10): Both ports closed, (Center), Resilience τ_β (14): Both ports open, and (Right) Combination of stabilization of pneumatics and resilience $\Delta p_V \cdot \tau_\beta$ with both ports closed, which finds the right balance between partially contradictory design guidelines.

Actuation

Pneumatic Modes

With the default scenario portrayed in Figure 1, the inlets of the reservoirs for the aqueous reagent and the ancillary liquid are vented during rotation ($\omega > 0$), which can be interpreted as $V_0 \mapsto \infty$ and $V_0' \mapsto \infty$ in (10), and thus $\Delta p_V \mapsto 0$ (10). So as long as the centrifugally induced pressure head remains

positive, i.e., $\Delta p_\omega > 0$ (5) for $z < \mathcal{Z}$, the meniscus will reach $z \geq \mathcal{Z}$, and thus open DF at the outlet. However, especially for multiplexed flow control [103, 105], it is advantageous to create a critical spin rate

$$\Omega = \sqrt{\frac{p_V' - p_V}{\varrho \bar{r} \Delta r - \varrho' \bar{r}' \Delta r'}} \tag{15}$$

which first needs to be surpassed, i.e., $\omega > \Omega$, before trigging reagent release. In such centrifugo-pneumatic actuation, the ambient pressure p_0 applies to open, and p_V and p_V' (9) to sealed ports.

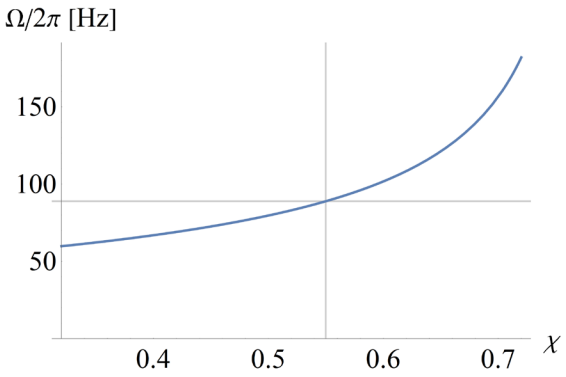

Figure 5 Burst frequency $\Omega/2\pi$ required to establish $z = \mathcal{Z}$ when both inlet ports remain sealed during rotation when reducing the ancillary volume U' by a factor of χ. Towards $\chi \mapsto 1$, Ω reaches values that are way out of reach for typical LoaD instruments, thus effectively preventing release. Yet, spin rates below the practical upper limit $\omega/2\pi \approx 100$ Hz can be achieved below $\chi \approx 0.55$. Default parameters (Table A1) are used, except that the cross sections $\mathcal{A}$ and a of the isoradial channel have been reduced by a factor of 3 to still assure its complete filling.

As the default experimental parameters $\varrho, \varrho', U, U', R$ and Γ (Table A1) are geared to result in $\Delta p_\omega = 0$ (5) at $z = \mathcal{Z}$, and thus $\Omega \mapsto \infty$, centrifugo-pneumatic actuation requires adjusting some of them. In general, the digital twin allows to determine the changes required to within the rather complex correlation between $\varrho, \varrho', U, U', R, \Gamma$ and Ω in order realize certain design targets. The example portrayed in Figure 5 shows the scaling of the critical spin rate $\Omega/2\pi$ (15) with the ancillary volume $\chi \cdot U'$. Spindle speeds $\Omega/2\pi$ (15) within the experimentally achievable range not surpassing about 100 Hz only emerge below $\chi \approx 0.55$. Note that in order to make sure that the isoradial channel is always filled with the ancillary liquid, the cross sections $\mathcal{A}$ and a are both reduced by a factor of 3 with respect to the values in Table A1.

Note that equation (10) also discloses $\Delta p_V \propto p_0$. This scaling with the atmospheric pressure p_0 only affects the overall magnitude of Δp_V, but not the direction and ratio of the pneumatic pressures. We therefore refer to previous work on centrifugo-pneumatic valving where the impact and possible compensation of variation in the atmospheric pressure by weather, and particularly local altitude, have been examined in more detail [27, 98, 103, 105].

The critical spin rate Ω (15) also determines the maximum (density) of the centrifugal field $f_\omega = \varrho_{\mathrm{part}} \cdot R_{\mathrm{LUO}} \cdot \Omega^2$ that can be sustained by the reagent valve, e.g., while an LUO such as plasma extraction is simultaneously processed to separate blood cells of (relative) density ϱ_{part} at $\omega < \Omega \pm M \cdot \Delta\Omega$.

Systematic Volume Losses

Due to related to evaporation or absorption at rates $\dot{U}$ and $\dot{U}'$, liquid volumes may appreciably decline during storage over time periods T, typically lasting months to a few years, by $\delta U = \dot{U} \cdot T$ and $\delta U' = \dot{U}' \cdot T$. Even for open inlet ports during rotation, the reduced volumes $U - \delta U$ and $U' - \delta U'$ may lead

to $\Delta p_\omega(\varrho, \varrho', U - \delta U, U' - \delta U', R, \Gamma, \mathcal{Z}) < 0$ (5), and thus valve malfunction by failing to dissolve the DF at $z = \mathcal{Z}$. (In addition, these losses may also affect the outcome of quantitative assays.)

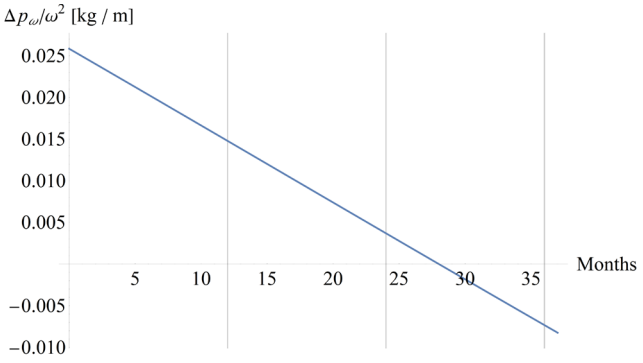

Figure 6 Systematic reductions $\delta U = \dot{U} \cdot T$ and $\delta U' = \dot{U}' \cdot T$ of the originally loaded liquid volumes U and U' at rates $\dot{U}$ and $\dot{U}'$ change the centrifugal pressure balance p_ω/ω^2 (6) over a time T. In this example, annual loss rates of $\dot{U}$ and $\dot{U}'$ of 5% and 1% are assumed, and $\dot{U} > \dot{U}'$ is compensated by loading 10% more reagent volume U. The curve shows that the opening condition $p_\omega/\omega^2 > 0$ is assured beyond a typical minimum storage period of 24 months.

The main impact of the liquid losses δU and $\delta U'$ on the density-weighted radial products $\bar{r}\Delta r$ and $\bar{r}'\Delta r'$ in the centrifugal equilibrium (6) is through $\Delta r = R - r$ and $\Delta r' = R - r'$ via $r(U, \delta U, A) = (U - \dot{U} \cdot T)/A$ and $r'(U', \delta U', A') = (U' - \dot{U}' \cdot T)/A'$. Enlarged cross sections A and A' thus mitigate the effect of evaporation or other losses of the reagent and ancillary phases at $\dot{U}$ and $\dot{U}'$. Figure 6 shows that the prerequisite $\Delta p_\omega > 0$ for $z = \mathcal{Z}$ is provided for nearly 2.5 years at exemplary annual evaporation losses of 5% and 1% for the reagent and the ancillary liquid, respectively. This condition of a positive centrifugal pressure differential Δp_ω (10) also implies that sufficient liquid volumes U and U' are at available for all interface locations $z_\mathcal{Z} \leq z \leq \mathcal{Z}$ to displace U_Δ (7) from the reagent side through the isoradial segment into the ancillary reservoir.

Statistical Tolerances

Consistent reagent release hinges upon $|\tilde{z}(\varrho, \varrho', U, U', R, \Gamma, \Delta\varrho, \Delta\varrho', \Delta U, \Delta U', \Delta R, \Delta\Gamma) - \mathcal{Z}| \leq M \cdot \Delta z(z = \mathcal{Z})$ in hydrostatic equilibrium (5) at $\omega > 0$. The standard deviation Δz (8) is governed by the unavoidable spreads $\{\Delta\gamma_k\}$ of the experimental input parameters $\{\gamma_k\}$, mainly in the geometrical dimensions $\Delta\Gamma$ and ΔU defining the structure Γ and the loaded liquid volumes U and U', respectively. The histogram in Figure 7 displays the distribution of $\tilde{z}$ with a mean $\bar{z} = 19.97$ mm close to $\mathcal{Z} = 20$ mm and a standard deviation $\Delta z = 4.02$ mm (8) obtained from a Monte-Carlo simulation with 1000 runs using the default values and realistic tolerances Δd and Δw in vertical and lateral machining, and pipetting the liquid volumes ΔU and $\Delta U'$ as listed in Table A1.

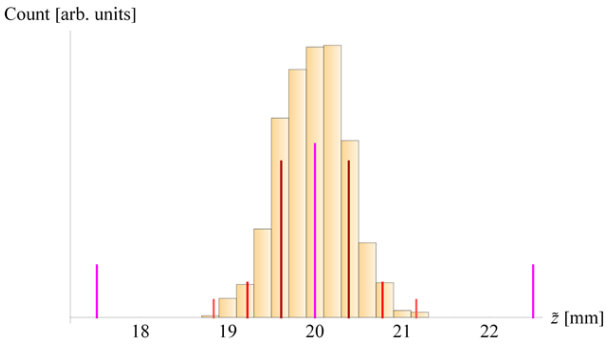

Figure 7 Monte-Carlo simulation of the distribution of actual meniscus position $\tilde{z}$ when targeting $z = \mathcal{Z} = 20$ mm a centrifugal equilibrium $\Delta p_\omega = 0$ obtained with the default parameters $\varrho, \varrho', U, U', R$ and Γ while factoring in their respective tolerances $\Delta U, \Delta U'$ and $\Delta\Gamma$ (Table A1). After 1000 (time consuming) runs, the histogram features a mean position $\bar{z} = 19.99$ mm with a standard deviation $\Delta z = 0.387$ mm. The vertical lines indicate (magenta) the default

center and limits of the DF at $z = \mathcal{Z}, \mathcal{Z} \pm 0.5 \cdot \delta\mathcal{Z}$, respectively, and (red shades) $z = \mathcal{Z} \pm M \cdot \Delta z$ with $M = \{1,2,3\}$ with the standard deviation Δz (8) of the $\tilde{z}$-distribution.

Gas Enclosure

During priming or storage, bubbles may emerge within the liquids. For developing a semi-quantitative understanding of their influence on valving, we consider the case of a gas of volume $V_{\mathrm{g},0}$ entrapped at ambient pressure p_0 in the center of the -isoradial $\mathcal{z}$-segment after loading. Upon reaching equilibrium during spinning at $\omega > 0$, the original volume $V_{\mathrm{g},0}$ is compressed to

$$V_{\mathrm{g}}(\omega) = V_{\mathrm{g},0} \cdot \frac{p_0}{p_0 + p_\omega} = V_{\mathrm{g},0} \cdot \frac{p_0}{p_0 + \varrho \cdot \bar{r}\Delta r \cdot \omega^2} \tag{16}$$

while now residing at $z = \mathcal{Z}$. To still open the DF in presence of the entrapped gas, the liquid volumes U and U' need to be sized so that the meniscus at z would have to be shifted by a further $0.5 \cdot V_{\mathrm{g}}(\omega)/\mathcal{A}$ (16) in the isoradial z-axis compared to the absence of a bubble. (Alternatively, the position $\mathcal{Z}$ can be appropriately adjusted to provide bubble tolerance.)

Assuming symmetrical displacement into each lateral reservoir (which is, strictly speaking, only the case for $\varrho = \varrho'$), the liquid levels r and r' in hydrostatic equilibrium (5) are lifted by about $0.5 \cdot V_{\mathrm{g}}(\omega)/A$ and $0.5 \cdot V_{\mathrm{g}}(\omega)/A'$ towards the center of rotation, respectively. The impact of such a gas enclosure is assessed in a back-ot-the-envelope calculation; for this, we assume $V_0 = 1\ \mu\mathrm{l}$, $p_0 = p_{\mathrm{std}}$, $\nu = \omega/2\pi = 25\ \mathrm{Hz}$ and default values for the other parameters (Table A1), to arrive at typical values of $V \approx 0.9\, V_{\mathrm{g},0}$ and $\delta r \approx \delta r' \approx 1\ \mathrm{mm}$.

Refinements

In order to illustrate the concept and potential of a digital twin for optimizing the long-term storage and release mechanism towards strategic design goals, we introduced a simple structure Γ (Figure 1); this way, engineering objectives could be quantified and expressed by algebraic equations, which can be solved on reasonable time scales by commonly available computing power.

Pegging the forward meniscus of the first introduced liquid by a small capillary barrier, sometimes also referred to as phase guide, at $z = \mathcal{z}$, is amongst many possible improvements. A possible trapping of an interstitial bubble after filling the second liquid may be prevented by a gas permeable membrane, located near $z = \mathcal{z}$, or a local outlet to be sealed after priming has completed. Stiction, e.g., caused by capillary pinning to manufacturing-related artefacts or dust, may be overcome by choosing a sufficiently high spin rate $\omega \gg 0$ for reaching hydrostatic equilibrium (5) at $z = \mathcal{Z}$.

To avoid possible interference of with the assay protocol, the ancillary liquid might be cleanly removed under prevalent laminar flow conditions through an additional side pocket and centrifugal stratification. The permanently gas filled parts of reservoirs may be placed at distal locations as long as they are still pneumatically connected through conduits, e.g., to make efficient use of precious disc real estate required for multiplexed assay panels. The pneumatic seals may also be removed through secondary mechanism, e.g., akin to venting procedures implemented for centrifugo-pneumatic valves based on mechanical [76], laser- [82, 106] or pneumatic [37, 66, 86, 88-91, 105-112] principles.

Summary and Outlook

Summary

A novel technology has been introduced for Lab-on-a-Disc systems which offers a physical evaporation barrier and stabilization of liquid distributions during long-term storage, transport, and handling. Reagent release proceeds through a dissolvable film disintegrating upon centrifugally induced contact with the aqueous reagent. The complex interdependencies governing the operational principle over

its multiparameter space have been modelled to characterize system robustness and behavior *in silico*. The resulting digital twin further enables computational design optimization towards given performance objectives within practically achievable ranges regimes of experimental input parameters. In addition, systematic volume losses, e.g., through evaporation during storage, artefacts like enclosed gas bubbles, and statistical deviations in experimental input parameters can be factored in.

Outlook

Evidently, the work presented represents the blueprint for setting up digital twins to efficiently characterize and improve other functional elements of (centrifugal) microfluidic Lab-on-a-Disc systems. Its simplified representation of the valving structure by cuboidal elements can be significantly refined to optimize flow, e.g., by curved contours of the compartments, their inclination with respect to the radial orientation, and fins to guide the relocation of liquids and gases. Similar to the entrapped bubble, further parasitic effects observed during experimental testing, and additional elements of the layout can be included in the digital twin. Such enhancements will require a more complex computational fluid dynamic (CFD) simulation, which should also include inertia of the liquid and elastic components such as the sealing membranes, which may bend or even yield under pressure.

It is well known that tests with real systems will show effects that are not included in the digital-twin modelling. So, it is well expected that experimental validation will remain a substantial tool for arriving at a product. However, in particular during early stage of development where manufacturing and testing is mostly manual, only very limited numbers of fluidic chips are available, which usually prevent collecting sufficient statistics for proper device performance and reliability analysis. The digital twin presented in this work can then efficiently expedite design iteration of microfluidic systems by providing virtual prototyping and testing. Such a tool hence empowers failure mode and effects analysis (FMEA) regarding unavoidable tolerances, and *in silico* optimization of the layout for given design targets. Adding similar programs for simulating manufacturing and biochemical processes would also be desirable to combine with the digital twin for fluidics presented here.

On the bigger picture, the digital twin concept can boost microfluidic industries by standardization [113-115], interpreted in a way that validated boundary conditions issued by foundries can incorporated in computational design software to guarantee manufacturability and acceptable performance within given cost limits. Moreover, the digital twin modelling published here lends itself for open platform concepts in an increasingly digitized world, which can leverage crowdsourcing of brains, hands, infrastructure and equipment, e.g., coordinated by the rapidly emerging, decentralized blockchain technology [116-119].

Appendix

Table A1 Default dimensions and boundary conditions for experimental parameters of the valving structure Γ (Figure 1).

Isoradial Channel	$R = 30$ mm	$\mathcal{L} = 30$ mm	$\mathcal{H} = 3$ mm
Isoradial z-Segment	$z = 10$ mm	$\delta z = 5$ mm	$\hbar = 2$ mm
DF Region	$\mathcal{Z} = 15$ mm	$\delta\mathcal{Z} = 5$ mm	
Cross Sections (depth × width)	$A = 1$ mm × 10 mm	$A' = 1$ mm × 10 mm	$\mathcal{A} = 1$ mm × 3 mm
	$a = 1$ mm × 5 mm	$a' = 1$ mm × 4.5 mm	$\mathcal{a} = 1$ mm × 2 mm
Depths	$D = d = 1$ mm	$D' = d' = 1$ mm	$\mathcal{D} = \mathcal{d} = 1$ mm
Reservoir Heights	$H = 15$ mm	$H' = 10$ mm	
	$h = 5$ mm	$h' = 2.5$ mm	
Minimum Dimensions	Vertical ≥ 300 µm	Lateral ≥ 200 µm	Wall Thickness ≥ 1 mm

Structurable area:	$R_{\min} = 7.5\ \mathrm{mm}$	$R_{\max} = 55\ \mathrm{mm}$	
Geom. Tolerances	Vertical: 30 µm	Lateral: 20 µm	
Liquid Volumes	$U = 160\ \mu\mathrm{l}$	$U' \approx 60.68\ \mu\mathrm{l}$	$\Delta U = \Delta U' = 100\ \mathrm{nl}$
Minimum Filling Gap	$\delta H = \delta H' = 1\ \mathrm{mm}$		
Liquid Densities	$\varrho = 997\ \mathrm{kg \cdot m^{-3}}$	$\varrho' = 1680\ \mathrm{kg \cdot m^{-3}}$	
Liquid Viscosities	$\eta = 1.0016\ \mathrm{mPa \cdot s}$	$\eta' = 0.64\ \mathrm{mPa \cdot s}$	
Ambient pressure	$p_0 = p_{\mathrm{std}} = 1013.25\ \mathrm{hPa}$		

The default parameters of the basic structure Γ in Figure 1 are listed in Table A1. The default tolerances in vertical and lateral dimensions are $\Delta d = 30\ \mu\mathrm{m}$ and $\Delta w = 20\ \mu\mathrm{m}$, respectively. The minimum wall thickness between fluidic cavities is set to $1\ \mathrm{mm}$ to account for scale-up of production by injection molding, and sufficient surface bonding. The properties of water and "FC-72" (3M™ Fluorinert™ Electronic Liquid FC-72) representing an aqueous reagent and an immiscible ancillary liquid (at $25°\mathrm{C}$) are used. The volume of the ancillary fluid U' is chosen to settle $z = \mathcal{Z}$ at $\omega > 0$ (for both reservoirs open). For the definition of liquid volumes, $\Delta U = \Delta U' = 100\ \mathrm{nl}$ are assumed, and minimum gap δH between the filling level and the seal is implemented for facilitating loading. Fluctuations in p_0 with respect to the standard atmospheric pressure p_{std} are limited to the range following whether conditions, i.e., about 4%; the impact of the local altitude on p_0 is more pronounced when operating the LoaD in mountainous regions. The impact of variance in $\varrho, \varrho', z, \delta z, \mathcal{Z}, \delta\mathcal{Z}, \mathcal{L}$ and R on the meniscus position z is assumed to be neglectable.

References

1. Manz, A., N. Graber, and H.M. Widmer *Miniaturized total chemical analysis systems: A novel concept for chemical sensing*. Sensors and Actuators B: Chemical, 1990. **1**, 244-248 DOI: 10.1016/0925-4005(90)80209-I.
2. Auroux, P.-A., D. Iossifidis, D.R. Reyes, and A. Manz *Micro Total Analysis Systems. 2. Analytical Standard Operations and Applications*. Analytical Chemistry, 2002. **74**, 2637-2652 DOI: 10.1021/ac020239t.
3. Reyes, D.R., D. Iossifidis, P.-A. Auroux, and A. Manz *Micro Total Analysis Systems. 1. Introduction, Theory, and Technology*. Analytical Chemistry, 2002. **74**, 2623-2636 DOI: 10.1021/ac0202435.
4. Whitesides, G.M. *The origins and the future of microfluidics*. Nature, 2006. **442**, 368-373 DOI: 10.1038/nature05058.
5. Janasek, D., J. Franzke, and A. Manz *Scaling and the design of miniaturized chemical-analysis systems*. Nature, 2006. **442**, 374-380 DOI: 10.1038/nature05059.
6. Gijs, M.A.M., F. Lacharme, and U. Lehmann *Microfluidic Applications of Magnetic Particles for Biological Analysis and Catalysis*. Chemical Reviews, 2010. **110**, 1518-1563 DOI: 10.1021/cr9001929.
7. Nge, P.N., C.I. Rogers, and A.T. Woolley *Advances in Microfluidic Materials, Functions, Integration, and Applications*. Chemical Reviews, 2013. **113**, 2550-2583 DOI: 10.1021/cr300337x.
8. Liu, Q., C. Wu, H. Cai, N. Hu, J. Zhou, and P. Wang *Cell-Based Biosensors and Their Application in Biomedicine*. Chemical Reviews, 2014. **114**, 6423-6461 DOI: 10.1021/cr2003129.
9. Mauk, M., J. Song, H.H. Bau, R. Gross, F.D. Bushman, R.G. Collman, and C. Liu *Miniaturized devices for point of care molecular detection of HIV*. Lab on a Chip, 2017. **17**, 382-394 DOI: 10.1039/c6lc01239f.
10. Yuan, X. and R.D. Oleschuk *Advances in Microchip Liquid Chromatography*. Analytical Chemistry, 2018. **90**, 283-301 DOI: 10.1021/acs.analchem.7b04329.
11. Olanrewaju, A., M. Beaugrand, M. Yafia, and D. Juncker *Capillary microfluidics in microchannels: from microfluidic networks to capillaric circuits*. Lab on a Chip, 2018. **18**, 2323-2347 DOI: 10.1039/c8lc00458g.

12. Schembri, C.T., V. Ostoich, P.J. Lingane, T.L. Burd, and S.N. Buhl *Portable Simultaneous Multiple Analyte Whole-Blood Analyzer for Point-of-Care Testing*. Clinical Chemistry, 1992. **38**, 1665-1670 DOI: 10.1093/clinchem/38.9.1665.
13. Schembri, C.T., T.L. Burd, A.R. Kopfsill, L.R. Shea, and B. Braynin *Centrifugation and Capillarity Integrated into a Multiple Analyte Whole-Blood Analyzer*. Journal of Automatic Chemistry, 1995. **17**, 99-104 DOI: 10.1155/S1463924695000174.
14. *Abaxis (Piccolo Express)*. Accessed: 14/06/2021; Available on: https://www.abaxis.com/.
15. Andersson, P., G. Jesson, G. Kylberg, G. Ekstrand, and G. Thorsen *Parallel nanoliter microfluidic analysis system*. Analytical Chemistry, 2007. **79**, 4022-4030 DOI: 10.1021/ac061692y.
16. Inganas, M., H. Derand, A. Eckersten, G. Ekstrand, A.K. Honerud, G. Jesson, G. Thorsen, T. Soderman, and P. Andersson *Integrated microfluidic compact disc device with potential use in both centralized and point-of-care laboratory settings*. Clinical Chemistry, 2005. **51**, 1985-7 DOI: 10.1373/clinchem.2005.053181.
17. *Gyros Protein Technologies*. Accessed: 14/06/2021; Available on: https://www.gyrosproteintechnologies.com/.
18. Madou, M.J. and G.J. Kellogg *The LabCD (TM): A centrifuge-based microfluidic platform for diagnostics*. Systems and Technologies for Clinical Diagnostics and Drug Discovery, Proceedings Of, 1998. **3259**, 80-93 DOI: 10.1117/12.307314.
19. Shea, M. *ADMET Assays on Tecan's LabCD-ADMET System*. Journal of the Association for Laboratory Automation, 2003. **8**, 74-77 DOI: 10.1016/s1535-5535(04)00260-6.
20. Smith, S., D. Mager, A. Perebikovsky, E. Shamloo, D. Kinahan, R. Mishra, S.M.T. Delgado, H. Kido, S. Saha, J. Ducrée, M. Madou, K. Land, and J.G. Korvink *CD-Based Microfluidics for Primary Care in Extreme Point-of-Care Settings*. Micromachines, 2016. **7**, DOI: 10.3390/mi7020022.
21. Kong, L.X., A. Perebikovsky, J. Moebius, L. Kulinsky, and M. Madou *Lab-on-a-CD: A Fully Integrated Molecular Diagnostic System*. Journal of the Association for Laboratory Automation, 2016. **21**, 323-355 DOI: 10.1177/2211068215588456.
22. Maguire, I., R. O'Kennedy, J. Ducrée, and F. Regan *A review of centrifugal microfluidics in environmental monitoring*. Analytical Methods, 2018. **10**, 1497-1515 DOI: 10.1039/c8ay00361k.
23. Gorkin, R., J. Park, J. Siegrist, M. Amasia, B.S. Lee, J.M. Park, J. Kim, H. Kim, M. Madou, and Y.K. Cho *Centrifugal microfluidics for biomedical applications*. Lab on a Chip, 2010. **10**, 1758-1773 DOI: 10.1039/b924109d.
24. Burger, R., L. Amato, and A. Boisen *Detection methods for centrifugal microfluidic platforms*. Biosensors and Bioelectronics, 2016. **76**, 54-67 DOI: 10.1016/j.bios.2015.06.075.
25. Aeinehvand, M.M., F. Ibrahim, W. Al-Faqheri, K. Joseph, and M.J. Madou *Recent advances in the development of micropumps, microvalves and micromixers and the integration of carbon electrodes on centrifugal microfluidic platforms*. International Journal of Nanotechnology, 2018. **15**, 53-68 DOI: 10.1504/IJNT.2018.089559.
26. Sciuto, E.L., S. Petralia, G. Calabrese, and S. Conoci *An integrated biosensor platform for extraction and detection of nucleic acids*. Biotechnol Bioeng, 2020. DOI: 10.1002/bit.27290.
27. Ducrée, J. *Design optimization of centrifugal microfluidic "Lab-on-a-Disc" systems towards fluidic larger-scale integration*. Appled Sciences, 2021. **11**, 5839 DOI: 10.3390/app11135839.
28. Ramachandraiah, H., M. Amasia, J. Cole, P. Sheard, S. Pickhaver, C. Walker, V. Wirta, P. Lexow, R. Lione, and A. Russom, *Lab-on-DVD: standard DVD drives as a novel laser scanning microscope for image based point of care diagnostics.* Lab Chip, 2013. **13**(8): p. 1578-85.
29. Thompson, B.L., C. Birch, D.A. Nelson, J. Li, J.A. DuVall, D. Le Roux, A.C. Tsuei, D.L. Mills, B.E. Root, and J.P. Landers *A centrifugal microfluidic device with integrated gold leaf electrodes for the electrophoretic separation of DNA*. Lab on a Chip, 2016. **16**, 4569-4580 DOI: 10.1039/c6lc00953k.

30. Krauss, S.T., M.S. Woolf, K.C. Hadley, N.M. Collins, A.Q. Nauman, and J.P. Landers *Centrifugal microfluidic devices using low-volume reagent storage and inward fluid displacement for presumptive drug detection*. Sensors and Actuators B: Chemical, 2019. **284**, 704-710 DOI: 10.1016/j.snb.2018.12.113.
31. Abi-Samra, K., L. Clime, L. Kong, R. Gorkin, T.H. Kim, Y.K. Cho, and M. Madou *Thermo-pneumatic pumping in centrifugal microfluidic platforms*. Microfluidics and Nanofluidics, 2011. **11**, 643-652 DOI: 10.1007/s10404-011-0830-5.
32. Thompson, B.L., R.J. Gilbert, M. Mejia, N. Shukla, D.M. Haverstick, G.T. Garner, and J.P. Landers *Hematocrit analysis through the use of an inexpensive centrifugal polyester-toner device with finger-to-chip blood loading capability*. Analytica Chimica Acta, 2016. **924**, 1-8 DOI: 10.1016/j.aca.2016.04.028.
33. Watts, A.S., A.A. Urbas, E. Moschou, V.G. Gavalas, J.V. Zoval, M. Madou, and L.G. Bachas *Centrifugal microfluidics with integrated sensing microdome optodes for multiion detection*. Analytical Chemistry, 2007. **79**, 8046-8054 DOI: 10.1021/ac0709100.
34. Kim, T.H., K. Abi-Samra, V. Sunkara, D.K. Park, M. Amasia, N. Kim, J. Kim, H. Kim, M. Madou, and Y.K. Cho, *Flow-enhanced electrochemical immunosensors on centrifugal microfluidic platforms.* Lab on a Chip, 2013. **13**(18): p. 3747-3754.
35. Moschou, E.A., A.D. Nicholson, G.Y. Jia, J.V. Zoval, M.J. Madou, L.G. Bachas, and S. Daunert, *Integration of microcolumns and microfluidic fractionators on multitasking centrifugal microfluidic platforms for the analysis of biomolecules.* Analytical and Bioanalytical Chemistry, 2006. **385**(3): p. 596-605.
36. Mark, D., S. Haeberle, T. Metz, S. Lutz, J. Ducrée, R. Zengerle, and F. von Stetten *Aliquoting structure for centrifugal microfluidics based on a new pneumatic valve*. MEMS 2008: 21st Ieee International Conference on Micro Electro Mechanical Systems, Technical Digest, 2008. 611-+.
37. Keller, M., S. Wadle, N. Paust, L. Dreesen, C. Nuese, O. Strohmeier, R. Zengerle, and F. von Stetten *Centrifugo-thermopneumatic fluid control for valving and aliquoting applied to multiplex real-time PCR on off-the-shelf centrifugal thermocycler*. RSC Advances, 2015. **5**, 89603-89611 DOI: 10.1039/c5ra16095b.
38. Grumann, M., A. Geipel, L. Riegger, R. Zengerle, and J. Ducrée *Batch-mode mixing on centrifugal microfluidic platforms*. Lab on a Chip, 2005. **5**, 560-5 DOI: 10.1039/b418253g.
39. Ducrée, J., T. Brenner, S. Haeberle, T. Glatzel, and R. Zengerle *Multilamination of flows in planar networks of rotating microchannels*. Microfluidics and Nanofluidics, 2006. **2**, 78-84 DOI: 10.1007/s10404-005-0056-5.
40. Burger, R., D. Kinahan, H. Cayron, N. Reis, J. Garcia da Fonseca, and J. Ducrée *Siphon-induced droplet break-off for enhanced mixing on a centrifugal platform*. Inventions, 2020. **5**, DOI: 10.3390/inventions5010001.
41. Ducrée, J., S. Haeberle, T. Brenner, T. Glatzel, and R. Zengerle *Patterning of flow and mixing in rotating radial microchannels*. Microfluidics and Nanofluidics, 2006. **2**, 97-105 DOI: 10.1007/s10404-005-0049-4.
42. Strohmeier, O., S. Keil, B. Kanat, P. Patel, M. Niedrig, M. Weidmann, F. Hufert, J. Drexler, R. Zengerle, and F. von Stetten *Automated nucleic acid extraction from whole blood, B. subtilis, E. coli, and Rift Valley fever virus on a centrifugal microfluidic LabDisk*. RSC Advances, 2015. **5**, 32144-32150 DOI: 10.1039/c5ra03399c.
43. Brassard, D., M. Geissler, M. Descarreaux, D. Tremblay, J. Daoud, L. Clime, M. Mounier, D. Charlebois, and T. Veres *Extraction of nucleic acids from blood: unveiling the potential of active pneumatic pumping in centrifugal microfluidics for integration and automation of sample preparation processes*. Lab on a Chip, 2019. **19**, 1941-1952 DOI: 10.1039/c9lc00276f.
44. Karle, M., J. Miwa, G. Roth, R. Zengerle, and F. von Stetten *A Novel Microfluidic Platform for Continuous DNA Extraction and Purification Using Laminar Flow Magnetophoresis*. IEEE 22nd

International Conference on Micro Electro Mechanical Systems (MEMS 2009), 2009. 276-279 DOI: 10.1109/Memsys.2009.4805372.
45. Kido, H., M. Micic, D. Smith, J. Zoval, J. Norton, and M. Madou *A novel, compact disk-like centrifugal microfluidics system for cell lysis and sample homogenization*. Colloids and Surfaces B-Biointerfaces, 2007. **58**, 44-51 DOI: 10.1016/j.colsurfb.2007.03.015.
46. Haeberle, S., T. Brenner, R. Zengerle, and J. Ducrée *Centrifugal extraction of plasma from whole blood on a rotating disk*. Lab on a Chip, 2006. **6**, 776-781 DOI: 10.1039/b604145k.
47. Steigert, J., T. Brenner, M. Grumann, L. Riegger, S. Lutz, R. Zengerle, and J. Ducrée *Integrated siphon-based metering and sedimentation of whole blood on a hydrophilic lab-on-a-disk*. Biomedical Microdevices, 2007. **9**, 675-679 DOI: 10.1007/s10544-007-9076-0.
48. Kinahan, D.J., S.M. Kearney, N.A. Kilcawley, P.L. Early, M.T. Glynn, and J. Ducrée *Density-Gradient Mediated Band Extraction of Leukocytes from Whole Blood Using Centrifugo-Pneumatic Siphon Valving on Centrifugal Microfluidic Discs*. PLOS ONE, 2016. **11**, e0155545 DOI: 10.1371/journal.pone.0155545.
49. Dimov, N., J. Gaughran, D. Mc Auley, D. Boyle, D.J. Kinahan, and J. Ducrée *Centrifugally Automated Solid-Phase Purification of RNA*. 2014 IEEE 27th International Conference on Micro Electro Mechanical Systems (MEMS), 2014. 260-263 DOI: 10.1109/MEMSYS.2014.6765625.
50. Gaughran, J., D. Boyle, J. Murphy, R. Kelly, and J. Ducrée *Phase-selective graphene oxide membranes for advanced microfluidic flow control*. Microsystems and Nanoengineering, 2016. **2**, 16008 DOI: 10.1038/micronano.2016.8.
51. Zehnle, S., M. Rombach, R. Zengerle, F. von Stetten, and N. Paust *Network simulation-based optimization of centrifugopneumatic blood plasma separation*. Biomicrofluidics, 2017. **11**, DOI: 10.1063/1.4979044.
52. Haeberle, S., R. Zengerle, and J. Ducrée *Centrifugal generation and manipulation of droplet emulsions*. Microfluidics and Nanofluidics, 2007. **3**, 65-75 DOI: 10.1007/s10404-006-0106-7.
53. Schuler, F., F. Schwemmer, M. Trotter, S. Wadle, R. Zengerle, F. von Stetten, and N. Paust *Centrifugal step emulsification applied for absolute quantification of nucleic acids by digital droplet RPA*. Lab on a Chip, 2015. **15**, 2759-2766 DOI: 10.1039/c5lc00291e.
54. Schuler, F., M. Trotter, M. Geltman, F. Schwemmer, S. Wadle, E. Dominguez-Garrido, M. Lopez, C. Cervera-Acedo, P. Santibanez, F. von Stetten, R. Zengerle, and N. Paust *Digital droplet PCR on disk*. Lab on a Chip, 2016. **16**, 208-216 DOI: 10.1039/c5lc01068c.
55. Czilwik, G., S.K. Vashist, V. Klein, A. Buderer, G. Roth, F. von Stetten, R. Zengerle, and D. Mark, *Magnetic chemiluminescent immunoassay for human C-reactive protein on the centrifugal microfluidics platform.* Rsc Advances, 2015. **5**(76): p. 61906-61912.
56. Grumann, M., A. Geipel, L. Riegger, R. Zengerle, and J. Ducrée, *Magneto-hydrodynamic micromixing for centrifugal lab-on-a-disk platforms*, in *Micro Total Analysis Systems 2004, Vol 1*. 2005. p. 593-595
57. Ducrée, J., S. Haeberle, S. Lutz, S. Pausch, F. von Stetten, and R. Zengerle *The centrifugal microfluidic Bio-Disk platform*. Journal of Micromechanics and Microengineering, 2007. **17**, S103-S115 DOI: 10.1088/0960-1317/17/7/S07.
58. Lutz, S., D. Mark, G. Roth, R. Zengerle, and F. von Stetten *Centrifugal Microfluidic Platforms for Molecular Diagnostics*. Clinical Chemistry and Laboratory Medicine, 2011. **49**, S608-S608.
59. Tang, M., G. Wang, S.-K. Kong, and H.-P. Ho *A Review of Biomedical Centrifugal Microfluidic Platforms*. Micromachines, 2016. **7**, DOI: 10.3390/mi7020026.
60. Duffy, D.C., H.L. Gillis, J. Lin, N.F. Sheppard, and G.J. Kellogg *Microfabricated Centrifugal Microfluidic Systems: Characterization and Multiple Enzymatic Assays*. Analytical Chemistry, 1999. **71**, 4669-4678 DOI: 10.1021/ac990682c.
61. Azimi-Boulali, J., M. Madadelahi, M.J. Madou, and S.O. Martinez-Chapa *Droplet and Particle Generation on Centrifugal Microfluidic Platforms: A Review*. Micromachines, 2020. **11**, DOI: 10.3390/mi11060603.

62. Strohmeier, O., M. Keller, F. Schwemmer, S. Zehnle, D. Mark, F. von Stetten, R. Zengerle, and N. Paust *Centrifugal microfluidic platforms: Advanced unit operations and applications*. Chemical Society Reviews, 2015. **44**, 6187-229 DOI: 10.1039/c4cs00371c.
63. Kong, L.X., A. Perebikovsky, J. Moebius, L. Kulinsky, and M. Madou *Lab-on-a-CD*. Journal of Laboratory Automation, 2016. **21**, 323-355 DOI: 10.1177/2211068215588456.
64. Aeinehvand, M.M., P. Magaña, M.S. Aeinehvand, O. Aguilar, M.J. Madou, and S.O. Martinez-Chapa *Ultra-rapid and low-cost fabrication of centrifugal microfluidic platforms with active mechanical valves*. RSC Advances, 2017. **7**, 55400-55407 DOI: 10.1039/c7ra11532f.
65. Aeinehvand, M.M., L. Weber, M. Jiménez, A. Palermo, M. Bauer, F.F. Loeffler, F. Ibrahim, F. Breitling, J. Korvink, M. Madou, D. Mager, and S.O. Martínez-Chapa *Elastic reversible valves on centrifugal microfluidic platforms*. Lab on a Chip, 2019. **19**, 1090-1100 DOI: 10.1039/C8LC00849C.
66. Hess, J.F., S. Zehnle, P. Juelg, T. Hutzenlaub, R. Zengerle, and N. Paust *Review on pneumatic operations in centrifugal microfluidics*. Lab on a Chip, 2019. **19**, 3745-3770 DOI: 10.1039/C9LC00441F.
67. Nguyen, H.V., V.D. Nguyen, H.Q. Nguyen, T.H.T. Chau, E.Y. Lee, and T.S. Seo *Nucleic acid diagnostics on the total integrated lab-on-a-disc for point-of-care testing*. Biosensors and Bioelectronics, 2019. **141**, 111466 DOI: 10.1016/j.bios.2019.111466.
68. Rombach, M., S. Hin, M. Specht, B. Johannsen, J. Lüddecke, N. Paust, R. Zengerle, L. Roux, T. Sutcliffe, J.R. Peham, C. Herz, M. Panning, O. Donoso Mantke, and K. Mitsakakis *RespiDisk: A point-of-care platform for fully automated detection of respiratory tract infection pathogens in clinical samples*. The Analyst, 2020. **145**, 7040-7047 DOI: 10.1039/d0an01226b.
69. Homann, A.R., L. Niebling, S. Zehnle, M. Beutler, L. Delamotte, M.-C. Rothmund, D. Czurratis, K.-D. Beller, R. Zengerle, H. Hoffmann, and N. Paust *A microfluidic cartridge for fast and accurate diagnosis of Mycobacterium tuberculosis infections on standard laboratory equipment*. Lab on a Chip, 2021. DOI: 10.1039/d1lc00035g.
70. Madadelahi, M., L.F. Acosta-Soto, S. Hosseini, S.O. Martinez-Chapa, and M.J. Madou *Mathematical modeling and computational analysis of centrifugal microfluidic platforms: A review*. Lab on a Chip, 2020. **20**, 1318-1357 DOI: 10.1039/c9lc00775j.
71. Miyazaki, C.M., E. Carthy, and D.J. Kinahan *Biosensing on the Centrifugal Microfluidic Lab-on-a-Disc Platform*. Processes, 2020. **8**, 1360 DOI: 10.3390/pr8111360.
72. Rombach, M., S. Hin, M. Specht, B. Johannsen, J. Lüddecke, N. Paust, R. Zengerle, L. Roux, T. Sutcliffe, J.R. Peham, C. Herz, M. Panning, O. Donoso Mantke, and K. Mitsakakis, *RespiDisk: a point-of-care platform for fully automated detection of respiratory tract infection pathogens in clinical samples.* The Analyst, 2020. **145**(21): p. 7040-7047.
73. Brennan, D., H. Coughlan, E. Clancy, N. Dimov, T. Barry, D. Kinahan, J. Ducrée, T.J. Smith, and P. Galvin *Development of an on-disc isothermal in vitro amplification and detection of bacterial RNA*. Sensors and Actuators, B: Chemical, 2017. **239**, 235-242 DOI: 10.1016/j.snb.2016.08.018.
74. Delgado, S.M.T., D.J. Kinahan, F.S. Sandoval, L.A.N. Julius, N.A. Kilcawley, J. Ducrée, and D. Mager *Fully automated chemiluminescence detection using an electrified-Lab-on-a-Disc (eLoaD) platform*. Lab on a Chip, 2016. **16**, 4002-4011 DOI: 10.1039/c6lc00973e.
75. Mishra, R., J. Gaughran, D. Kinahan, and J. Ducrée *Functional Membranes for Enhanced Rotational Flow Control on Centrifugal Microfluidic Platforms*. Reference Module in Materials Science and Materials Engineering, 2017. DOI: 10.1016/b978-0-12-803581-8.04041-8.
76. Kinahan, D.J., P.L. Early, A. Vembadi, E. MacNamara, N.A. Kilcawley, T. Glennon, D. Diamond, D. Brabazon, and J. Ducrée *Xurography actuated valving for centrifugal flow control*. Lab on a Chip, 2016. **16**, 3454-3459 DOI: 10.1039/c6lc00568c.
77. *SpinX Technologies*. Accessed: 15/06/2021; Available on: https://web.archive.org/web/20040414090409/http://www.spinx-technologies.com/.

78. Abi-Samra, K., R. Hanson, M. Madou, and R.A. Gorkin *Infrared controlled waxes for liquid handling and storage on a CD-microfluidic platform*. Lab on a Chip, 2011. **11**, 723-726 DOI: 10.1039/c0lc00160k.
79. Kong, L.X., K. Parate, K. Abi-Samra, and M. Madou *Multifunctional wax valves for liquid handling and incubation on a microfluidic CD*. Microfluidics and Nanofluidics, 2015. **18**, 1031-1037 DOI: 10.1007/s10404-014-1492-x.
80. Al-Faqheri, W., F. Ibrahim, T.H.G. Thio, J. Moebius, K. Joseph, H. Arof, and M. Madou *Vacuum/Compression Valving (VCV) Using Parrafin-Wax on a Centrifugal Microfluidic CD Platform*. PLOS ONE, 2013. **8**, DOI: 10.1371/journal.pone.0058523.
81. García-Cordero, J.L., F. Benito-Lopez, D. Diamond, J. Ducrée, and A.J. Ricco *Low-Cost Microfluidic Single-Use Valves and on-Board Reagent Storage Using Laser-Printer Technology*. IEEE 22nd International Conference on Micro Electro Mechanical Systems (MEMS 2009), 2009. 439-442 DOI: 10.1109/Memsys.2009.4805413.
82. García-Cordero, J.L., D. Kurzbuch, F. Benito-Lopez, D. Diamond, L.P. Lee, and A.J. Ricco *Optically addressable single-use microfluidic valves by laser printer lithography*. Lab on a Chip, 2010. **10**, 2680-7 DOI: 10.1039/c004980h.
83. Torres Delgado, S.M., D.J. Kinahan, L.A. Nirupa Julius, A. Mallette, D.S. Ardila, R. Mishra, C.M. Miyazaki, J.G. Korvink, J. Ducrée, and D. Mager *Wirelessly powered and remotely controlled valve-array for highly multiplexed analytical assay automation on a centrifugal microfluidic platform*. Biosensors and Bioelectronics, 2018. **109**, 214-223 DOI: 10.1016/j.bios.2018.03.012.
84. Clime, L., D. Brassard, M. Geissler, and T. Veres *Active pneumatic control of centrifugal microfluidic flows for lab-on-a-chip applications*. Lab on a Chip, 2015. **15**, 2400-2411 DOI: 10.1039/c4lc01490a.
85. Clime, L., J. Daoud, D. Brassard, L. Malic, M. Geissler, and T. Veres *Active pumping and control of flows in centrifugal microfluidics*. Microfluidics and Nanofluidics, 2019. **23**, DOI: 10.1007/s10404-019-2198-x.
86. Kinahan, D.J., S.M. Delgado, L.A.N. Julius, A. Mallette, D. Saenz-Ardila, R. Mishra, C.M. Miyazaki, J. Korvink, D. Mager, and J. Ducrée, *Wireless Closed-Loop Control of Centrifugo-Pneumatic Valving Towards Large-Scale Microfluidic Process Integration*, in *2018 IEEE Micro Electro Mechanical Systems (MEMS)*. 2018: Belfast, Northern Ireland. p. 1213-1216 DOI: 10.1109/MEMSYS.2018.8346781.
87. Delgado, S.M.T., D.J. Kinahan, L.A.N. Julius, A. Mallette, D.S. Ardila, R. Mishra, C.M. Miyazaki, J.G. Korvink, J. Ducrée, and D. Mager *Wirelessly powered and remotely controlled valve-array for highly multiplexed analytical assay automation on a centrifugal microfluidic platform*. Biosensors & Bioelectronics, 2018. **109**, 214-223 DOI: 10.1016/j.bios.2018.03.012.
88. Godino, N., R. Gorkin, 3rd, A.V. Linares, R. Burger, and J. Ducrée *Comprehensive integration of homogeneous bioassays via centrifugo-pneumatic cascading*. Lab on a Chip, 2013. **13**, 685-94 DOI: 10.1039/c2lc40722a.
89. Schwemmer, F., T. Hutzenlaub, D. Buselmeier, N. Paust, F. von Stetten, D. Mark, R. Zengerle, and D. Kosse *Centrifugo-pneumatic multi-liquid aliquoting-parallel aliquoting and combination of multiple liquids in centrifugal microfluidics*. Lab on a Chip, 2015. **15**, 3250-3258 DOI: 10.1039/c5lc00513b.
90. Zhao, Y., F. Schwemmer, S. Zehnle, F. von Stetten, R. Zengerle, and N. Paust *Centrifugo-pneumatic sedimentation, re-suspension and transport of microparticles*. Lab on a Chip, 2015. **15**, 4133-4137 DOI: 10.1039/c5lc00508f.
91. Zehnle, S., F. Schwemmer, R. Bergmann, F. von Stetten, R. Zengerle, and N. Paust *Pneumatic siphon valving and switching in centrifugal microfluidics controlled by rotational frequency or rotational acceleration*. Microfluidics and Nanofluidics, 2015. **19**, 1259-1269 DOI: 10.1007/s10404-015-1634-9.

92. Henderson, B.D., D.J. Kinahan, J. Rio, R. Mishra, D. King, S.M. Torres-Delgado, D. Mager, J.G. Korvink, and J. Ducrée *Siphon-Controlled Automation on a Lab-on-a-Disc Using Event-Triggered Dissolvable Film Valves*. Biosensors, 2021. **11**, DOI: 10.3390/1108103.
93. Gorkin, R., 3rd, C.E. Nwankire, J. Gaughran, X. Zhang, G.G. Donohoe, M. Rook, R. O'Kennedy, and J. Ducrée *Centrifugo-pneumatic valving utilizing dissolvable films*. Lab on a Chip, 2012. **12**, 2894-902 DOI: 10.1039/c2lc20973j.
94. Kinahan, D.J., S.M. Kearney, N. Dimov, M.T. Glynn, and J. Ducrée *Event-triggered logical flow control for comprehensive process integration of multi-step assays on centrifugal microfluidic platforms*. Lab on a Chip, 2014. **14**, 2249-58 DOI: 10.1039/c4lc00380b.
95. Kinahan, D.J., S.M. Kearney, O.P. Faneuil, M.T. Glynn, N. Dimov, and J. Ducrée *Paper imbibition for timing of multi-step liquid handling protocols on event-triggered centrifugal microfluidic lab-on-a-disc platforms*. RSC Advances, 2015. **5**, 1818-1826 DOI: 10.1039/c4ra14887h.
96. Mishra, R., R. Alam, D.J. Kinahan, K. Anderson, and J. Ducrée, *Lipophilic-Membrane Based Routing for Centrifugal Automation of Heterogeneous Immunoassays*, in *2015 28th IEEE International Conference on Micro Electro Mechanical Systems (MEMS 2015)*. 2015: Estoril, Portugal. p. 523-526 DOI: 10.1109/MEMSYS.2015.7051007.
97. Schwemmer, F., S. Zehnle, D. Mark, F. von Stetten, R. Zengerle, and N. Paust *A microfluidic timer for timed valving and pumping in centrifugal microfluidics*. Lab on a Chip, 2015. **15**, 1545-1553 DOI: 10.1039/C4LC01269K.
98. Ducrée, J. *Anti-counterfeit technologies for microfluidic "Lab-on-a-Disc" systems*. 2021. DOI: 10.20944/preprints202107.0443.v1.
99. Lu, Y., R. Mishra, D. McAuley, D. Boyle, and J. Ducrée, *Reliable liquid reagent storage and rotational release for centrifugal sample-to-answer automation*, in *Proceedings of the 24th International Conference on Miniaturized Systems for Chemistry and Life Sciences (µTAS 2020), October 04–08*, S.L.G.a.H. Lu, Editor. 2020, The Chemical and Biological Microsystems Society (CBMS): Virtual. p. 134-135
100. Mishra, R., D. McAuley, N. Rolinska, D. Boyle, and J. Ducrée, *Barrier-film based reagent storage and release on microfluidic platforms for sample-to-answer automation of bioassays*, in *Proceedings of the 24th International Conference on Miniaturized Systems for Chemistry and Life Sciences (µTAS 2020)*, S.L.G.a.H. Lu, Editor. 2020, The Chemical and Biological Microsystems Society (CBMS): Virtual. p. 382-383
101. *Digital Twin*. 2021; Accessed: 25/05/2021; Available on: https://en.wikipedia.org/wiki/Digital_twin.
102. Marr, B. *What Is Digital Twin Technology - And Why Is It So Important?* 2017 Published: 06/03/2017; Accessed: 25/05/2021; Available on: https://www.forbes.com/sites/bernardmarr/2017/03/06/what-is-digital-twin-technology-and-why-is-it-so-important/.
103. Ducrée, J. *Systematic review of centrifugal valving based on digital twin modelling towards highly integrated Lab-on-a-Disc systems*. Nature Microsystems & Nanoengineering, 2021. DOI: 10.20944/preprints202105.0683.v2.
104. Ducrée, J. *Efficient development of integrated Lab-On-A-Chip systems featuring operational robustness and nanufacturability*. Micromachines, 2019. **10**, 12 DOI: 10.3390/mi10120886.
105. Ducrée, J. *Secure air traffic control at the hub of multiplexing on the centrifugo-pneumatic Lab-on-a-Disc platform*. Micromachines, 2021. **12**, 700 DOI: 10.3390/mi12060700.
106. Mishra, R., G. Reilly, M. Agnew, A. Garvey, C. Rogers, E. Andrade, H. Ma, S. Fitzgerald, J. Zapatero, R. O'Kennedy, and J. Ducrée, *Laser-Actuated Centrifugo-Pneumatic Flow Control Towards 'Sample-to-Answer' Integrated Detection of Multi-Marker Panels at the Point-of-Care*, in *2018 IEEE Micro Electro Mechanical Systems (MEMS)*. 2018: Belfast, Northern Ireland. p. 1185-1188 DOI: 10.1109/MEMSYS.2018.8346774.
107. Godino, N., R. Gorkin, A.V. Linares, R. Burger, and J. Ducrée, *A Centrifugo-Pneumatic Cascade for Fully Integrated and Multiplexed Biological Analysis*, in *2012 IEEE 25th International*

Conference on Micro Electro Mechanical Systems (MEMS). 2012: Paris, France DOI: 10.1109/MEMSYS.2012.6170352.
108. Gorkin, R., L. Clime, M. Madou, and H. Kido, *Pneumatic pumping in centrifugal microfluidic platforms.* Microfluidics and Nanofluidics, 2010. **9**(2-3): p. 541-549.
109. Gorkin, R., C. Nwankire, J. Siegrist, R. Burger, J. Gaughran, and J. Ducree, *Rotationally controlled centrifugo-pneumatic valving utilizing dissolvable films*, in *2011 16th International Solid-State Sensors, Actuators and Microsystems Conference*. 2011. p. 1276-1279 DOI: 10.1109/transducers.2011.5969448.
110. Kinahan, D.J., M. Renou, D. Kurzbuch, N.A. Kilcawley, E. Bailey, M.T. Glynn, C. McDonagh, and J. Ducrée *Baking Powder Actuated Centrifugo-Pneumatic Valving for Automation of Multi-Step Bioassays*. Micromachines, 2016. **7**, DOI: 10.3390/mi7100175.
111. Mark, D., S. Haeberle, T. Metz, S. Lutz, J. Ducrée, R. Zengerle, and F. von Stetten *Aliquoting structure for centrifugal microfluidics based on a new pneumatic valve*. MEMS 2008: 21st IEEE International Conference on Micro Electro Mechanical Systems, Technical Digest, 2008. 611-614 DOI: 10.1109/MEMSYS.2008.4443730.
112. Mark, D., T. Metz, S. Haeberle, S. Lutz, J. Ducrée, R. Zengerle, and F. von Stetten *Centrifugo-pneumatic valve for metering of highly wetting liquids on centrifugal microfluidic platforms*. Lab on a Chip, 2009. **9**, 3599-3603 DOI: 10.1039/b914415c.
113. van Heeren, H. *Standards for connecting microfluidic devices?* Lab on a Chip, 2012. **12**, 1022-1025 DOI: 10.1039/C2LC20937C.
114. Stavis, S.M. *A glowing future for lab on a chip testing standards*. Lab on a Chip, 2012. **12**, 3008-11 DOI: 10.1039/c2lc40511c.
115. Reyes, D.R., H.v. Heeren, S. Guha, L.H. Herbertson, A.P. Tzannis, J. Ducrée, H. Bissig, and H. Becker *Accelerating Innovation and Commercialization Through Standardization of Microfluidic-Based Medical Devices*. Lab on a Chip, 2021. **21**, 9-21 DOI: 10.1039/D0LC00963F.
116. Ducrée, J., M. Gravitt, R. Walshe, S. Bartling, M. Etzrodt, and T. Harrington *Open Platform Concept for Blockchain-Enabled Crowdsourcing of Technology Development and Supply Chains*. Frontiers in Blockchain, 2020. **3**, 386525 DOI: 10.3389/fbloc.2020.586525.
117. Ducrée, J., M. Etzrodt, B. Gordijn, M. Gravitt, S. Bartling, R. Walshe, and T. Harrington *Blockchain for Organising Effective Grass-Roots Actions on a Global Commons: Saving The Planet*. Frontiers in Blockchain, 2020. **3**, 33 DOI: 10.3389/fbloc.2020.00033.
118. Ducrée, J., M. Etzrodt, S. Bartling, R. Walshe, T. Harrington, N. Wittek, S. Posth, K.W.A. Ionita, W. Prinz, D. Kogias, T. Paixão, I. Peterfi, and J. Lawton *Unchaining collective intelligence for science, research and technology development by blockchain-boosted community participation*. Frontiers in Blockchain, 2021. DOI: 10.3389/fbloc.2021.631648.
119. Ducrée, J. *Research - A blockchain of knowledge?* Blockchain - Research and Applications, 2020. **1**, 100005 DOI: 10.1016/j.bcra.2020.100005.